Discovery of Charge Order and Corresponding Edge State in Kagome Magnet FeGe

Jia-Xin Yin, Yu-Xiao Jiang, Xiaokun Teng, Md. Shafayat Hossain, Sougata Mardanya, Tay-Rong Chang, Zijin Ye, Gang Xu, M. Michael Denner, Titus Neupert, Benjamin Lienhard, Han-Bin Deng, Chandan Setty, Qimiao Si, Guoqing Chang, Zurab Guguchia, Bin Gao, Nana Shumiya, Qi Zhang, Tyler A. Cochran, Daniel Multer, Ming Yi, Pengcheng Dai, and M. Zahid Hasan

Phys. Rev. Lett. **129**, 166401 — Published 10 October 2022

DOI: 10.1103/PhysRevLett.129.166401

Discovery of charge order and corresponding edge state in kagome magnet FeGe

Authors: Jia-Xin Yin[1]*†, Yu-Xiao Jiang[1]*, Xiaokun Teng[2]*, Md. Shafayat Hossain[1], Sougata Mardanya[3], Tay-Rong Chang[3], Zijin Ye[4], Gang Xu[4], M. Michael Denner[5], Titus Neupert[5], Benjamin Lienhard[6], Han-Bin Deng[7], Chandan Setty[2], Qimiao Si[2], Guoqing Chang[8], Zurab Guguchia[9], Bin Gao[2], Nana Shumiya[1], Qi Zhang[1], Tyler A. Cochran[1], Daniel Multer[1], Ming Yi[2], Pengcheng Dai[2], M. Zahid Hasan[1,10,11,12]†

Affiliations:

[1]Laboratory for Topological Quantum Matter and Advanced Spectroscopy (B7), Department of Physics, Princeton University, Princeton, New Jersey 08544, USA.

[2]Department of Physics and Astronomy, Rice Center for Quantum Materials, Rice University, Houston, Texas 77005, USA.

[3]Department of Physics, National Cheng Kung University, Tainan 70101, Taiwan.

[4]Wuhan National High Magnetic Field Center & School of Physics, Huazhong University of Science and Technology, Wuhan 430074, China.

[5]Department of Physics, University of Zurich, Winterthurerstrasse 190, 8057 Zurich, Switzerland.

[6]Department of Electrical Engineering and Computer Science, Massachusetts Institute of Technology, Cambridge, MA 02139, USA.

[7]Beijing National Laboratory for Condensed Matter Physics and Institute of Physics, Chinese Academy of Sciences, Beijing 100190, China.

[8]Division of Physics and Applied Physics, School of Physical and Mathematical Sciences, Nanyang Technological University, Singapore 639798, Singapore.

[9]Laboratory for Muon Spin Spectroscopy, Paul Scherrer Institute, CH-5232 Villigen PSI, Switzerland.

[10]Lawrence Berkeley National Laboratory, Berkeley, California 94720, USA.

[11]Princeton Institute for the Science and Technology of Materials, Princeton University, Princeton, NJ 08544, USA

[12]Quantum Science Center, Oak Ridge, TN 37830, USA

†Corresponding authors, E-mail:

jiaxiny@princeton.edu; mzhasan@princeton.edu
*These authors contributed equally to this work.

Kagome materials often host exotic quantum phases, including spin liquids, Chern gap, charge density wave, and superconductivity. Existing scanning microscopy studies of the kagome charge order have been limited to non-kagome surface layers. Here we tunnel into the kagome lattice of FeGe to uncover features of the charge order. Our spectroscopic imaging identifies a 2×2 charge order in the magnetic kagome lattice, resembling that discovered in kagome superconductors. Spin-mapping across steps of unit-cell-height demonstrates the existence of spin-polarized electrons with an antiferromagnetic stacking order. We further uncover the correlation between antiferromagnetism and charge order anisotropy, highlighting the unusual magnetic coupling of the charge order. Finally, we detect a pronounced edge state within the charge order energy gap, which is robust against the irregular shape fluctuations of the kagome lattice edges. We discuss our results with the theoretically considered topological features of the kagome charge order including unconventional magnetism and bulk-boundary correspondence.

A kagome lattice, made of corner-sharing triangles, is a geometrically frustrated lattice first introduced to quantum physics [1] in 1951, while a similar pattern unit has long been used as the star of David in religious ceremony and as the Hexagram in alchemy symbols. With the recent advance of quantum materials, it has been demonstrated that kagome materials can support a variety of quantum phases, including spin liquids, Chern gap, charge density wave, and superconductivity, significantly promoting the diversity of quantum matter in a model lattice setting [1-6]. In contrast to other low-temperature phases, the kagome charge order can occur at high temperatures up to 100K exhibiting many-body correlations and Berry curvature physics. Recent theories [6-13] have proposed topological features of the kagome charge order, including orbital currents/magnetism, and bulk-boundary correspondence. Fundamentally, the charge order driven by the kagome van Hove singularities can induce a nontrivial Berry phase and accordingly various Berry phase related quantum effects [14], presenting a rare case of interaction-driven quantum topology explored in recent theories [15,16,17]. The many-body interaction not only opens a charge density wave gap at E_F, but also produces a nontrivial Berry phase that leads to orbital currents/magnetism and a topological edge state, as illustrated in Fig. 1(a) [7-13].

Scanning tunneling microscopy (STM) was among the first experimental techniques to discover the charge order in kagome superconductors AV_3Sb_5 (A=K, Rb, Cs). However, existing STM studies have been focused on the Sb honeycomb layers [7,18-26], rather than directly probing the kagome lattice layer. Notably, intriguing kagome physics may not be detected on the non-kagome surface layers [4,27,28], and features detected on non-kagome layers (such as surface stripe reconstructions) may also not be directly related to the kagome lattice. Therefore, tunneling directly into the kagome lattice is essential to probe the intrinsic features of the kagome charge order, and is particularly important to solving puzzles regarding different behaviors of the charge order on non-kagome surfaces [7, 18-26]. Recently, our combined neutron scattering [29], STM and photoemssion experiments on kagome antiferromagnet FeGe unexpectedly detected a superlattice signal around 100K, suggesting it likely to be a kagome charge order platform. According to the STM study on CoSn — a cousin material to FeGe — the atomic kagome lattice layer can be prepared as the surface termination through cryogenic cleaving [28], offering us an unprecedented opportunity to explore the kagome charge order at the microscopic level.

In this work, single crystals with a size up to 2mm × 2mm are cleaved in situ at 77K in ultra-high vacuum conditions and then inserted into the microscope head, already at ^{4}He base temperature (4.2K). Data are taken at 4.2K unless otherwise specified. Topographic images in this work are taken with the tunneling junction set-up $V = 60$mV and $I = 0.05$nA. Tunneling conductance spectra are obtained with an Ir/Pt tip using standard lock-in amplifier techniques with a lock-in frequency of 977Hz and a junction set-up of $V = 100 \sim 60$mV, $I = 1$nA, and a root mean square oscillation voltage of 0.5mV. Tunneling conductance maps are obtained with taking a spectrum at every location under a junction set-up of $V = 60$mV, $I = 0.3 \sim 0.1$nA, and a root mean square oscillation voltage of 5mV.

FeGe has a hexagonal structure (space group P6/mmm) with lattice constants $a = 5.0$ Å and $c = 4.0$ Å. It consists of a Fe_3Ge kagome layer and a Ge_2 honeycomb layer with alternating stacking [Fig. 1(b)]. Pioneering studies [30] have established it as a kagome antiferromagnet with a Neel transition over 400K. The spins of Fe kagome lattice are ordered predominantly along the *c*-axis, while a weak spin canting has been observed at low temperatures [30]. The cryogenic cleaving of 11 systems produces both the honeycomb lattice and kagome lattice layers as the natural terminations [Fig. 1(b)]. Figure 1(c) shows a case of a half-unit-cell step with a step height of 2.0Å, revealing both Ge_2 honeycomb layer and Fe_3Ge kagome layer. In this work, we focus on the kagome lattice, as shown in Fig. 1(d), and its inset. Similar to the cases in CoSn [28], and Fe_3Sn_2 [27,31], the individual atoms in the honeycomb layer can be well resolved, while the individual kagome atoms are often not easy to be resolved in the STM experiment. We further perform spectroscopic imaging on the kagome lattice, focusing on the Fermi-level electronic structure. The Fourier transform of the dI/dV map in Fig. 1(e) and its inset demonstrates the 2×2 vector peaks from the charge order in addition to the Bragg peaks of the lattice. The 2×2 vector peaks are consistent with the wave vector of bulk charge order obtained in our neutron study of FeGe. The three pairs of 2×2 vector peaks feature different intensities

as shown in Fig. 1(f), resembling the chiral charge order reported in the defect-free Sb surfaces in AV_3Sb_5. Counting from the highest to the lowest intensity vector peak pairs, we define an anticlockwise chirality [7,19,20,24] for this atomic region. At E_F, we also detected an energy gap with a size around 50meV [Fig. 1(g)]. Across this energy gap, a partial real-space charge density reversal is observed through spectroscopic imaging [Fig. 1(h) inset], as expected for a charge density wave order [7,34]. This gap disappears above the charge ordering temperature that is around 100K, together with the disappearance of the 2×2 vector peaks in the spectroscopic map data, as shown in Fig. 1(h) and its inset. These spectroscopic data sets establish the existence of charge order in the magnetic kagome lattice of FeGe.

An outstanding question is whether our observed charge order can be topological as proposed in several related theories [6-13]. STM can be used to examine the nontrivial consequences of topological phases. Theoretical treatment of chiral charge order often considers a winding phase (tied to its chirality) between the three sets of order parameters associated with three symmetry-related ordering vectors. This phase difference of the triple order parameters leads to orbital currents with a nontrivial Berry phase [Fig. 1(a)][6-13]. The associated Berry curvature field introduces a weak orbital magnetization with its direction tied to the chirality. Meanwhile, the proposed topological charge order can feature a bulk-boundary correspondence with edge states inside the bulk gap. Specifically, in the case of the antiferromagnet FeGe, one can expect that the weak orbital magnetization of the topological charge order can be polarized by the strong antiferromagnetic spin order, resulting in a chirality-switching charge order between adjacent kagome layers that our tunneling experiments can directly reveal.

To explore the interplay between charge order and dominant spin order in the kagome lattice, we perform spin-polarized tunneling. While spin-polarized tunneling signals have been detected in kagome ferromagnet [35,36], spin-polarized tunneling measurements are lacking for kagome antiferromagnets. One of the three ways for preparing magnetic probes is to dip the nonmagnetic tip into magnetic materials [37]. We find that progressively dipping the Pt/Ir tip into the magnetic kagome layer can effectively produce a magnetic tip. With this magnetic tip, we study a nearby region composed of kagome surfaces with unit-cell-height steps [Fig. 2(a)]. The spin-flip field for FeGe is known [29] to exceed 10T, beyond our instrumental capability, and thus we can safely determine that our low magnetic field only flips the spin of the magnetic tip. Figure 2(b) shows dI/dV maps taken at E_F for the same nano-region in Fig. 2(a) with the tip spin polarized in the up direction (upper panel) and down direction (down panel), respectively. In the upper panel, terraces ②④⑥ have a stronger intensity, while in the lower panel, terraces ①③⑤⑦ reveal a more prominent intensity. The intensity contrast and contrast reversal systematically provide key evidence for spin-polarized tunneling. Figure 2(c) compares the dI/dV signals for terraces ④ and ⑤ as sweeping *c*-axis magnetic field from -1T to +1T. A switch of their signals for positive and negative fields is obtained, and further indicates that the saturation field of the magnetic tip is around 0.4T. Our data sets suggest that the kagome lattice has strong spin-polarized states at E_F and the adjacent kagome layers have states with opposite dominant spin polarizations, which are fully consistent with the expected bulk antiferromagnetic spin order along the *c*-axis.

With the demonstration of antiferromagnetism of FeGe and the spin-resolving capability of our magnetic probe, we further characterize the magnetic features of the charge order. We zoom into the boxed area for terraces ④ and ⑤ and measure additional atomic-scale dI/dV maps with the tip spin polarized to opposite directions. We subtract the two maps taken with opposite tip polarizations to obtain the magnetic contrast map in Figs. 2(d) and (f) after carefully aligning their atomic positions. Both magnetic contrast maps show 2×2 modulations, as further evidenced by their Fourier transform in Figs. 2(e) and (g). While both magnetic contrast maps show 2×2 charge order, we find their chirality is evidently opposite to each other [Figs. 2(e) and (g)], thus defining an antichiral charge order. Theoretical proposals [6-13] of topological charge order often indicate (Berry curvature induced) weak orbital magnetism [38-40] whose direction is tied to the chirality of the underlying order parameter and the orbital magnetization moment can couple to either an external or internal magnetic field. In AV_3Sb_5, the applied magnetic

field can switch the chirality of the charge order. In contrast, in FeGe, the strong staggered internal magnetic field can cause switching of the chirality between different kagome layers. Such a magnetic coupling of the charge order is consistent with our neutron scattering observation [29] of additional enhancement of the magnetic moment just below the charge ordering temperature. In addition, the chirality switch of the charge order is similarly evidenced by using a nonmagnetic tip to image a unit cell step [Fig. 2(h)], further confirming our spin-polarized tunneling results.

Besides the orbital magnetism, theoretical studies [6-13] of the charge order also suggest the existence of boundary modes resulting from a topological charge order bulk gap. The bulk-boundary correspondence is a key concept in quantum topology [41]. In a topological material, the nontrivial bulk gap features gapless boundary states. Through extensive scanning searching, we can obtain unit-cell-height kagome step edges, as shown in Fig. 3(a). Spectroscopic imaging at E_F with a nonmagnetic tip at zero-field clearly demonstrates pronounced edge states for all these edges. The edge state is rather robust in that it is observed almost independently of the irregular shape of the edges, pointing to a protection mechanism. We do not detect edge states for energies outside the charge order gap, as demonstrated in the series of dI/dV mapping data in Fig. 3(b). The high-resolution dI/dV spectrum taken at the edge in Fig. 3(c) confirms the emergence of states only inside the charge order gap. We further show the spatial decay of the edge state towards the kagome lattice in Fig. 3(d). An exponential fitting of the decay curve estimates the characteristic decay length of 2.1nm. We also confirm that the edge state disappears above the charge ordering temperature, as shown in Fig. 3(e). Crucially, the emergence of robust edge states within the kagome lattice charge order gap is consistent with the bulk-boundary correspondence expected for a topological charge order proposed in several theoretical works [6-13]. Compared with the topological edge states [4,42-46] seen in other metallic systems, the edge states in FeGe uniquely emerge at the E_F. The emergence of Fermi-level edge states implies the charge-order-driven anomalous transverse transports, which is consistent with our observation of large anomalous Hall effect just below the charge ordering temperature [29] when giant magnetic fields are applied to overcome antiferromagnetism along the *c*-axis. Taken together with the magnetic coupling of the charge order supported by the spin-chirality correlation within each kagome layer, our tunneling work provides microscopic experimental data consistent with the orbital magnetism and bulk-boundary correspondence for the charge order in kagome magnet FeGe.

References:

1 I. Syôzi, *Statistics of kagomé lattice*, Prog. Theor. Phys. **6**, 306 (1951).

2 C. Broholm, R. J. Cava, S. A. Kivelson, D. G. Nocera, M. R. Norman, and T. Senthil, *Quantum spin liquids*, Science **367**, eaay0668 (2020).

3 J.-X. Yin, S. H. Pan, and M. Z. Hasan, *Probing topological quantum matter with scanning tunnelling microscopy*, Nat. Rev. Phys. **3**, 249 (2021).

4 J.-X. Yin *et al*., *Quantum-limit Chern topological magnetism in $TbMn_6Sn_6$*, Nature **583**, 533 (2020).

5 T. Neupert, M. M. Denner, J.-X. Yin, R. Thomale, and M. Z. Hasan, *Charge order and superconductivity in kagome materials*, Nat. Phys. **18**, 137 (2022).

6 K. Jiang, T. Wu, J.-X. Yin, Z. Wang, M. Z. Hasan, S. D. Wilson, X. Chen, and J. Hu, *Kagome superconductors AV_3Sb_5 (A=K, Rb, Cs)*, preprint at arXiv:2109.10809 (2021).

7 Y.-X. Jiang *et al*., *Unconventional chiral charge order in kagome superconductor KV_3Sb_5*, Nat. Mater. **20**, 1353 (2021).

8 X. Feng, K. Jiang, Z. Wang, and J. Hu, *Chiral flux phase in the Kagome superconductor AV_3Sb_5*, Sci. Bull. **66**, 1384 (2021).

9 M. M. Denner, R. Thomale, and T. Neupert, *Analysis of Charge Order in the Kagome Metal AV_3Sb_5 (A=K, Rb, Cs)*, Phys. Rev. Lett. **127**, 217601 (2021).

10 Y.-P. Lin and R. M. Nandkishore, *Complex charge density waves at Van Hove singularity on hexagonal lattices: Haldane-model phase diagram and potential realization in the kagome metals AV_3Sb_5 (A=K, Rb, Cs)*, Phys. Rev. B **104**, 045122 (2021).
11 T. Park, M. Ye, and L. Balents, *Electronic instabilities of kagome metals: saddle points and Landau theory*, Phys. Rev. B **104**, 035142 (2021).
12 C. Setty, H. Hu, L. Chen, and Q. Si, *Electron correlations and -breaking density wave order in a kagome metal*, preprint at arXiv:2105.15204 (2021).
13 S. Zhou and Z. Wang, *Chern Fermi-pockets and chiral topological pair density waves in kagome superconductors*, preprint at arXiv:2110.06266 (2022).
14 D. Xiao, M.-C. Chang, and Q. Niu, *Berry phase effects on electronic properties*, Rev. Mod. Phys. **82**, 1959 (2010).
15 F. D. M. Haldane, *Model for a quantum Hall effect without Landau levels: Condensed-matter realization of the" parity anomaly"*, Phys. Rev. Lett. **61**, 2015 (1988).
16 X. G. Wen, F. Wilczek, and A. Zee, *Chiral spin states and superconductivity*, Phys. Rev. B **39**, 11413 (1989).
17 C. M. Varma, *Non-Fermi-liquid states and pairing instability of a general model of copper oxide metals*, Phys. Rev. B **55**, 14554 (1997).
18 Z. Liang *et al*., *Three-Dimensional Charge Density Wave and Surface-Dependent Vortex-Core States in a Kagome Superconductor CsV_3Sb_5*, Phys. Rev. X **11**, 031026 (2021).
19 N. Shumiya *et al*., *Intrinsic nature of chiral charge order in the kagome superconductor RbV_3Sb_5*, Phys. Rev. B **104**, 035131 (2021).
20 Z. Wang *et al*., *Electronic nature of chiral charge order in the kagome superconductor CsV_3Sb_5*, Phys. Rev. B **104**, 075148 (2021).
21 H. Zhao, H. Li, B. R. Ortiz, S. M. L. Teicher, T. Park, M. Ye, Z. Wang, L. Balents, S. D. Wilson, and I. Zeljkovic, *Cascade of correlated electron states in the kagome superconductor CsV_3Sb_5*, Nature **599**, 216 (2021).
22 H. Chen *et al*., *Roton pair density wave in a strong-coupling kagome superconductor*, Nature **599**, 222 (2021).
23 H.-S. Xu, Y.-J. Yan, R. Yin, W. Xia, S. Fang, Z. Chen, Y. Li, W. Yang, Y. Guo, and D.-L. Feng, *Multiband Superconductivity with Sign-Preserving Order Parameter in Kagome Superconductor CsV_3Sb_5*, Phys. Rev. Lett. **127**, 187004 (2021).
24 C. Mielke III *et al*., *Time-reversal symmetry-breaking charge order in a kagome superconductor*, Nature **602**, 245 (2022).
25 H. Li, S. Wan, H. Li, Q. Li, Q. Gu, H. Yang, Y. Li, Z. Wang, Y. Yao, and H.-H. Wen, *No observation of chiral flux current in the topological kagome metal CsV_3Sb_5*, Phys. Rev. B **105**, 045102 (2022).
26 J. Yu *et al*., *Evolution of electronic structure in pristine and Rb-reconstructed surfaces of kagome metal RbV_3Sb_5*, Nano Lett. **22**, 918 (2022).
27 J.-X. Yin *et al*., *Giant and anisotropic many-body spin–orbit tunability in a strongly correlated kagome magnet*, Nature **562**, 91 (2018).
28 J.-X. Yin *et al*., *Fermion–boson many-body interplay in a frustrated kagome paramagnet*, Nat. Commun. **11**, 4003 (2020).
29 X. Teng *et al*., *Discovery of charge density wave in a kagome lattice antiferromagnet*, Nature (2022), DOI: 10.1038/s41586-022-05034-z.
30 J. Bernhard, B. Lebech, and O. Beckman, *Neutron diffraction studies of the low-temperature magnetic structure of hexagonal FeGe*, J. Phys. F: Met. Phys. **14**, 2379 (1984).
31 Z. Lin *et al*., *Flatbands and emergent ferromagnetic ordering in Fe_3Sn_2 kagome lattices*, Phys. Rev. Lett. **121**, 096401 (2018).

32 M. Kang *et al*., *Dirac fermions and flat bands in the ideal kagome metal FeSn*, Nat. Mater. **19**, 163 (2020).
33 B. C. Sales, J. Yan, W. R. Meier, A. D. Christianson, S. Okamoto, and M. A. McGuire, *Electronic, magnetic, and thermodynamic properties of the kagome layer compound FeSn*, Phys. Rev. Mater. **3**, 114203 (2019).
34 M. Spera, A. Scarfato, Á. Pásztor, E. Giannini, D. R. Bowler, and Ch. Renner, *Insight into the charge density wave gap from contrast inversion in topographic STM images*, Phys. Rev. Lett. **125**, 267603 (2020).
35 J.-X. Yin *et al*., *Spin-orbit quantum impurity in a topological magnet*, Nat. Commun. **11**, 4415 (2020).
36 Y. Xing *et al*., *Localized spin-orbit polaron in magnetic Weyl semimetal $Co_3Sn_2S_2$*, Nat. Commun. **11**, 5613 (2020).
37 R. Wiesendanger, *Spin mapping at the nanoscale and atomic scale*, Rev. Mod. Phys. **81**, 1495 (2009).
38 J.-X. Yin *et al*., *Negative flat band magnetism in a spin–orbit-coupled correlated kagome magnet*, Nat. Phys. **15**, 443 (2019).
39 C. L. Tschirhart *et al*., *Imaging orbital ferromagnetism in a moiré Chern insulator*, Science **372**, 1323 (2021).
40 H. Huang *et al*., *Flat-band-induced anomalous anisotropic charge transport and orbital magnetism in kagome metal CoSn*, Phys. Rev. Lett. **128**, 096601 (2022).
41 Y. Hatsugai, *Chern number and edge states in the integer quantum Hall effect*, Phys. Rev. Lett. **71**, 3697 (1993).
42 F. Yang *et al*., *Spatial and energy distribution of topological edge states in single Bi (111) bilayer*, Phys. Rev. Lett. **109**, 016801 (2012).
43 C. Pauly *et al*., *Subnanometre-wide electron channels protected by topology*, Nat. Phys. **11**, 338 (2015).
44 Z. Wang *et al*., *Topological edge states in a high-temperature superconductor FeSe/$SrTiO_3$ (001) film*, Nat. Mater. **15**, 968 (2016).
45 P. Sessi *et al*., *Robust spin-polarized midgap states at step edges of topological crystalline insulators*, Science **354**, 1269 (2016).
46 L. Peng, Y. Yuan, G. Li, X. Yang, J.-J. Xian, C.-J. Yi, Y.-G. Shi, and Y.-S. Fu, *Observation of topological states residing at step edges of WTe_2*, Nat. Commun. **8**, 659 (2017).

Acknowledgement:

M.Z.H. acknowledges support from the US Department of Energy, Office of Science, National Quantum Information Science Research Centers, Quantum Science Center and Princeton University. M.Z.H. acknowledges visiting scientist support at Berkeley Lab (Lawrence Berkeley National Laboratory) during the early phases of this work. Theoretical and STM works at Princeton University was supported by the Gordon and Betty Moore Foundation (GBMF9461; GBMF4547; M.Z.H.). The theoretical work including ARPES were supported by the US DOE under the Basic Energy Sciences program (grant number DOE/BES DE-FG-02-05ER46200; M.Z.H.). T.-R.C. was supported by the Young Scholar Fellowship Program under a MOST grant for the Columbus Program, MOST111-2636-M-006-014, the Higher Education Sprout Project, Ministry of Education to the Headquarters of University Advancement at the National Cheng Kung University (NCKU), the National Center for Theoretical Sciences (Taiwan). The work at Rice was supported by US NSF-DMR-2100741, the Robert A. Welch Foundation under grant no. C-1839, C-2024, and No. C-1411, the U.S. Department Of Energy (DOE) grant no. DE-SC0021421 and No. DE-SC0018197, and the Gordon and Betty Moore Foundation's EPiQS Initiative through grant no. GBMF9470. The work at Nanyang Technological University was supported by the National Research Foundation, Singa- pore under its Fellowship Award (NRF-NRFF13-2021-0010). T.N. acknowledges support from the European Union's Horizon 2020 research and innovation programme (ERC-StG-Neupert-757867-PARATOP). G. X. acknowledges support from the National Key Research and Development Program of China (2018YFA0307000), and the National Natural Science Foun- dation of China (11874022).

Figures

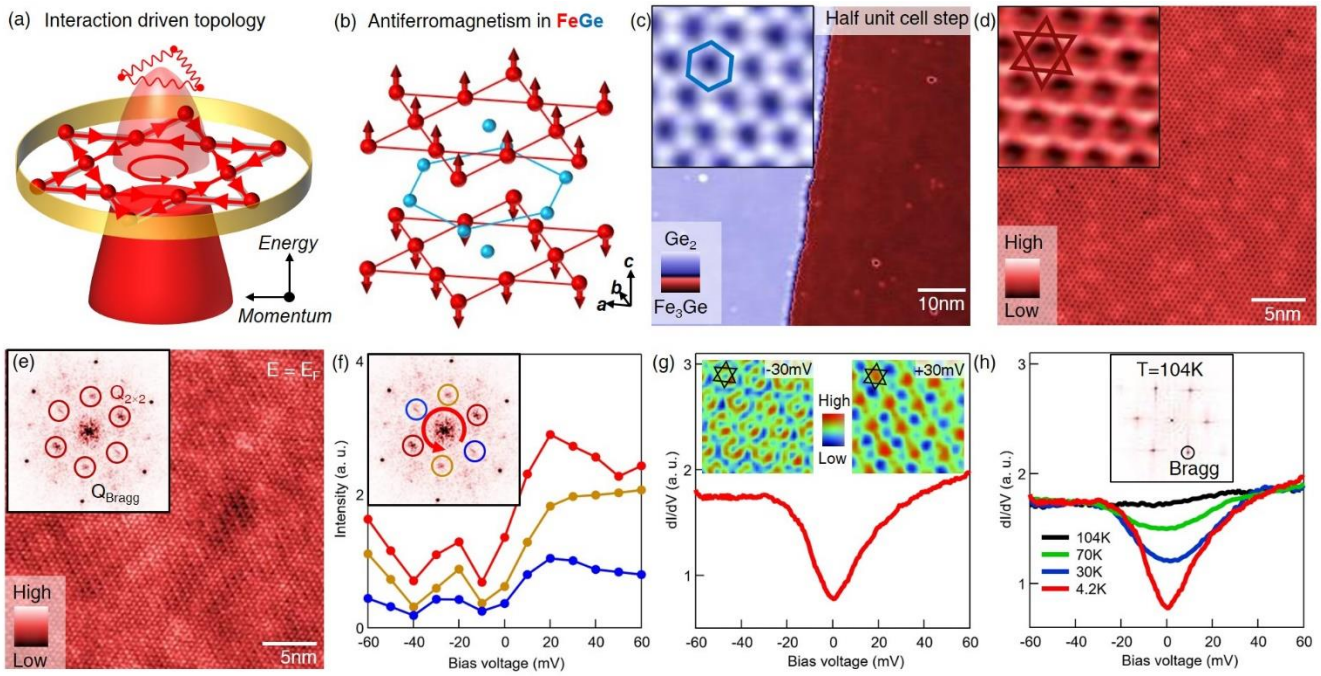

Fig 1. (a) Many-body interaction (red springs) driven topology in kagome lattice (red spheres). The interaction not only opens a charge density wave gap at E_F, but also produces a nontrivial Berry phase (red circular arrows) that leads to orbital currents/magnetism (thick red arrows) and a topological edge state (yellow ring). The light and dark red ellipsoid represent unoccupied and occupied electronic states, respectively. (b) Crystal structure of FeGe. The low temperature magnetic structure is an approximate A-type antiferromagnet. (c) Topographic image of a half unit cell step consisting of Ge and FeGe layers, and the zoom-in Ge layer marked with the honeycomb lattice (blue lines). (d) Topographic image of the kagome lattice layer of FeGe, and the zoomed-in image marked with the kagome lattice (red lines). (e) dI/dV map taken at E_F for the same kagome lattice region, and its Fourier transform identifying the 2×2 vector peaks. (f) Energy distribution of the three pairs of 2×2 vector peak intensities. Counting from the highest to the lowest intensity vector peak pairs, we define an anticlockwise chirality. (g) dI/dV spectrum taken on the kagome lattice, showing an energy gap. The insets show two tunneling current maps for the same region taken below and above this energy gap. We also mark the kagome lattice as black lines. The center of this marked kagome lattice shows a reversal of intensity for these two maps, consistent with a charge order. (h) Temperature dependence of tunneling spectrum showing the disappearance of energy gap at 104K, which is just above the charge ordering temperature. The inset shows the Fourier transform data of a dI/dV map taken at E_F at 104K, showing the disappearance of 2×2 vector peaks.

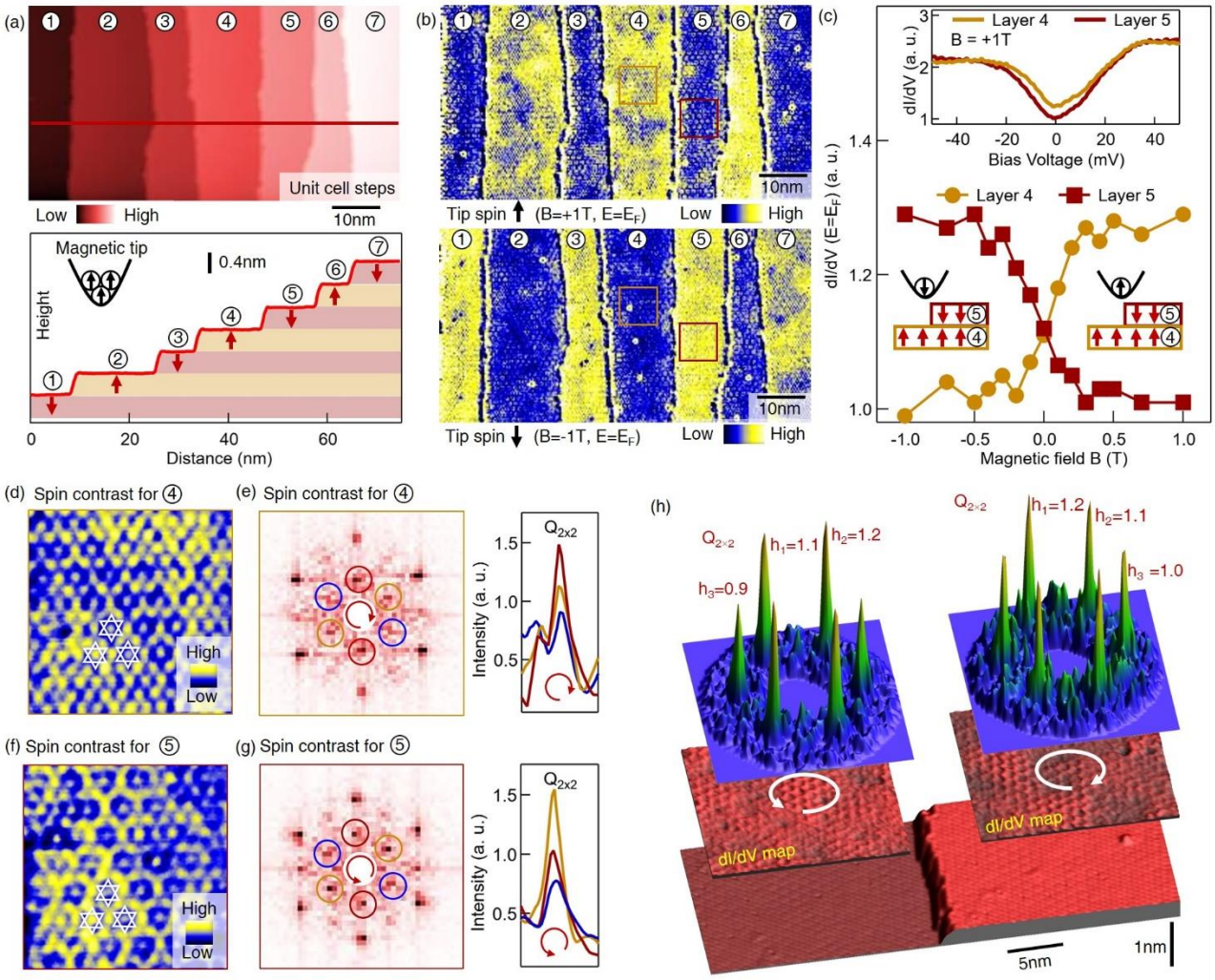

Fig 2. (a) Topographic image of kagome terraces with unit cell steps (upper panel) and their height profile (lower panel). A magnetic tip is used to obtain the data, and the kagome lattices are expected to couple antiferromagnetically along the c-axis. (b) dI/dV maps taken at E_F for the region in **a** with tip spin polarized in up (upper panel) and down (lower panel) directions. (c) dI/dV signal at E_F for kagome terrace ④ and ⑤ as a function of c-axis magnetic field sweeping. The lower inset shows the schetch illustrating spin configurations for the tip and sample at different magnetic fields. The upper inset shows the dI/dV data for kagome terrace ④ and ⑤ with B=+1T. (d) High-resolution dI/dV magnetic contrast data for terrace ④. The data is taken at the orange box region in (b), and obtained through subtracting +1T map with -1T map data. The white lines mark the 2×2 charge order. (e) Fourier transform of (d) showing 2×2 vector peaks. The right panel displays the intensity of the 2×2 vector peaks along the Bragg spot direction, from which we determine the clockwise chirality. (f) High-resolution dI/dV magnetic contrast data for terrace ⑤. The data is taken at the red box region in (b), and obtained through subtracting -1T map with +1T map data. (g) Fourier transform of (f) showing 2×2 vector peaks. The right panel displays the intensity of the 2×2 vector peaks along Bragg spot direction, from which we determine anticlockwise chirality. (h) Confirmation of the chirality switch with a nonmagnetic tip at zero field. The lower layer shows kagome lattices with a unit cell step. The middle layer shows dI/dV maps taken at E_F for the two terraces. The upper layer shows

the 2×2 vector peaks obtained by Fourier transforming the respective map data, from which we determine the opposite chirality for the two terraces.

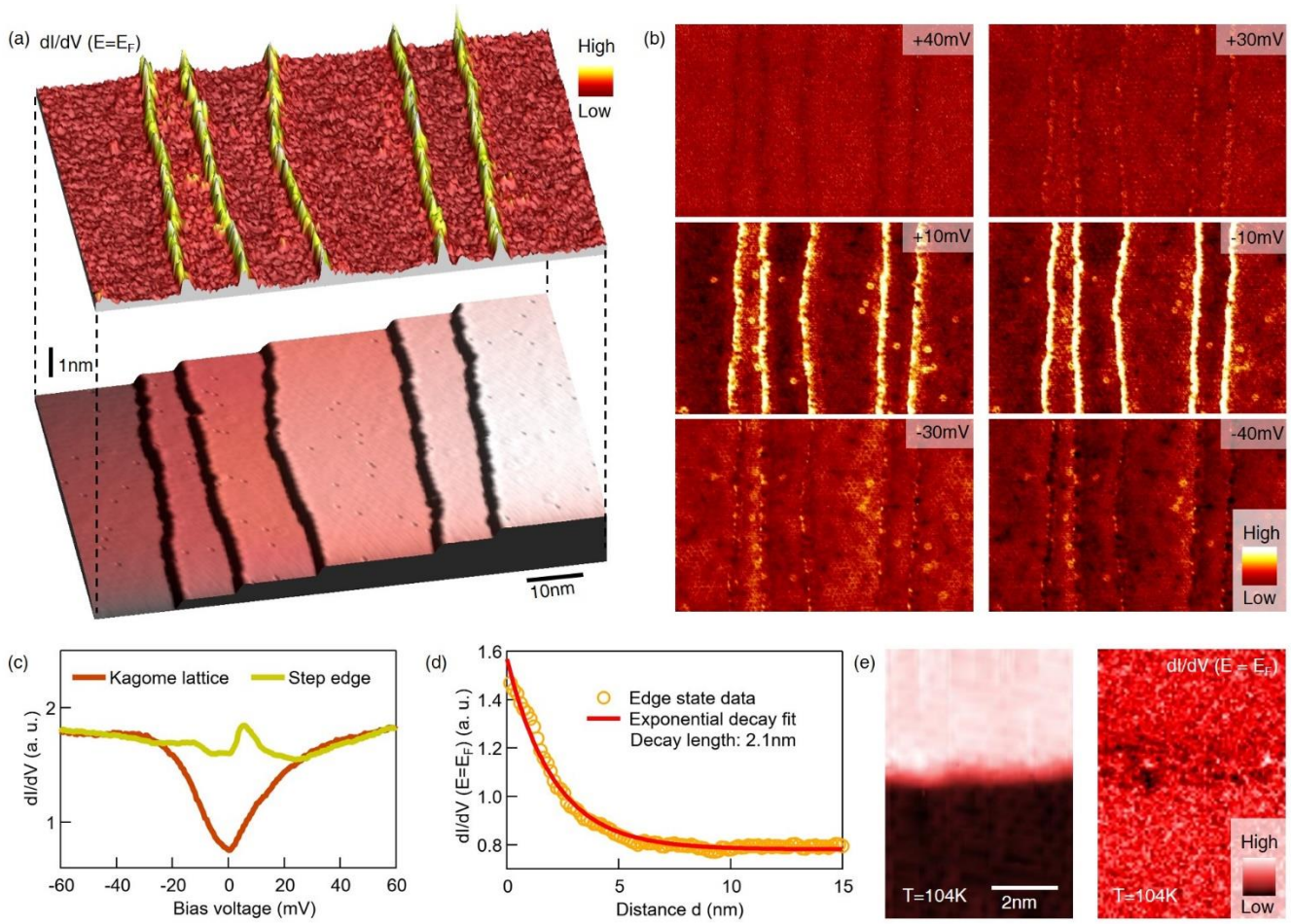

Fig 3. (a) dI/dV map taken at E_F (upper layer) for unit cell kagome step edges (lower layer), showing the robust edge states. (b) dI/dV maps taken for the same region at energies outside (upper and lower panels) and within (middle panels) the charge order energy gap. The kagome edge state appears only at the energies within the charge order energy gap. (c) dI/dV spectra taken at the kagome lattice and step edge, respectively. The step edge data shows the emergence of states within the charge order energy gap. (d) Spatial decay of the edge state. The decay can be fitted with an exponential function with a characteristic decay length of 2.1nm. (e) Topographic image of a unit cell kagome step edge (left) and its corresponding dI/dV map at Fermi energy taken at 104K, showing the disappearance of edge state above the charge ordering temperature that is around 100K.